07

# Influence of the grain boundary state on the plasticization effect in ultrafine-grained Al−0.4Zr alloy

© A.M. Mavlyutov[1,2], T.S. Orlova[1,¶], M.Yu. Murashkin[1,3], N.A. Enikeev[3]

[1] Ioffe Institute,
St. Petersburg, Russia
[2] St. Petersburg State University,
St. Petersburg, Russia
[3] Ufa University of Science and Technology,
Ufa, Russia

¶ E-mail: orlova.t@mail.ioffe.ru

*Received May 15, 2023*
*Revised July 18, 2023*
*Accepted July 20, 2023*

The influence of small additional deformation by cold rolling (CR) on the microstructure and mechanical properties of ultrafine-grained (UFG) Al−0.4Zr alloy structured by high pressure torsion (HPT) has been studied. The results are compared with the application of small additional deformation by HPT, which, after low-temperature annealing, leads to a substantial increase in ductility (plasticization effect) with small decrease in strength. It is shown that, in contrast to the additional deformation of HPT, the deformation of CR after intermediate low-temperature annealing leads to a sharp drop in plasticity to $\sim 2\%$, while the strength increases to $\sim 275$ MPa. The key role of the nonequilibrium state of grain boundaries in the manifestation of the plasticization effect in the UFG Al−0.4Zr alloy is revealed. A new approach is proposed for simultaneously increasing the strength and ductility of the UFG Al−0.4Zr alloy due to a small additional deformation by CR without intermediate annealing. As a result of this approach, a significant increase in strength by $\sim 30\%$ (ultimate tensile strength $\sim 223$ MPa) was achieved with a simultaneous increase in ductility up to $\sim 26\%$, which is associated with an increase in the strain hardening rate due to an increase in the density of lattice dislocations in the UFG structure with nonequilibrium grain boundaries. The strain rate sensitivity and strain hardening coefficients have been determined for the UFG Al−0.4Zr alloy in various states.

**Keywords:** aluminum-zirconium alloys, severe plastic deformation, ultrafine-grained structure, annealing-induced hardening, deformation-induced softening.

DOI: 10.61011/PSS.2023.09.57117.155

## 1. Introduction

Aluminium alloys are promising materials to be used as current-carrying conductors in overhead power lines (OHPL) [1]. The main disadvantage of aluminium alloys is their relatively low mechanical strength, therefore steel-reinforced aluminium wires are the most widely used materials for current-carrying conductors in OHPL. Steel core ensures reduced effective wire area and makes the manufacturing process more complicated [2]. Therefore, the search for solutions to improve the strength of aluminium wire alloys is an important challenge for electrical engineering. A promising method to improve the strength of electrical aluminium alloys involves material treatment by the severe plastic deformation (SPD) methods allowing to produce bulk samples with ultra-fine grained (UFG) or nanocrystalline (NC) structure [3]. Such structure ensures improved strength properties due to grain-boundary strengthening and strain hardening mechanisms [4]. Among the electrical aluminium alloys, Al−Zr system is of particular interest. Zirconium alloying in low concentrations (up to 1 wt.%) provides a structure resistant to temperature exposure [5–9].

Some studies achieved considerable improvement of strength for such alloys comparing with the conventional coarse–grained state by the treatment of SPD methods [10–13]. UFG alloys of the Al−Zr system produced by high-pressure torsion (HPT) have demonstrated the potential for operation in high temperature conditions [10,13]. However, small Zr additives only slightly improve the strength of aluminium in UFG condition [10,14]. In addition, grain refinement usually results in reduced plasticity of materials [3,4]. Therefore, production of wire materials with improved strength and significant plasticity at the same time is an important challenge for modern materials physics.

A recent study offered a new approach to improve plasticity of HPT-structured Al−0.4Zr (wt.%) UFG alloy [15]. This approach involved additional deformation-heat treatment (DHT), including short-term low-temperature annealing and small additional deformation by the HPT method. As a result a considerable plasticity improvement effect (plasticization effect (PE)) was found, which occurs in the UFG material and is not typical for traditional coarse-

grained materials. Similar effect has been observed earlier in UFG commercially pure aluminium [16,17]. For UFG Al, a model was offered to describe this effect by introducing additional dislocations into the high angle grain boundary structure relaxed by annealing [17,18].

To get deeper understanding of the physical nature of the plasticization effect in UFG Al−Zr alloys and to identify microstructural features controlling the manifestation of this effect, this study investigated the effect of an alternative type of additional deformation (cold rolling) and degree of additional deformation on PE in the HPT-structured Al−0.4Zr (wt.%) UFG alloy.

## 2. Study materials and experimental techniques

For the study, a material with the following chemical composition was chosen: 0.39Zr, 0.24Fe, 0.02Si, 0.02Zn, balance Al, wt.% (hereinafter referred to as Al−0.4Zr). The alloy was formed by combined casting and rolling (RUSAL, Moscow, Russia). The UFG structure was made by HPT treatment of the initial alloy at room temperature (RT) with 10 revolutions at 6 GPa. After such treatment, the samples had a disc shape with a diameter of 20 mm and a thickness of $\sim 1$ mm (hereinafter the samples are designated as HPT). The true deformation at a distance of 5 mm from the disc center was $\gamma \approx 6.6$ [3]. After the HPT treatment, some samples were annealed at 503 K during 1 h (HPT_AN state) and additionally cold rolled with 3% and 5% reduction (HPT_AN_CR state). Some samples were cold rolled immediately after the HPT treatment (HPT_CR state).

For uniaxial tension test, blade-shape samples with $6 \times 2$ mm test length were cut. The test was carried out at RT and a strain rate of $5 \cdot 10^{-4}\,s^{-1}$ using Shimadzu AG-XD Plus test machine. At least three samples were tested for each state. Additional uniaxial tension test was carried out with stepwise strain rate variation from $\dot{e} = 5 \cdot 10^{-4}\,s^{-1}$ to $\dot{e} = 1 \cdot 10^{-3}\,s^{-1}$ and a strain rate sensitivity coefficient ($m$) was calculated by the following relation [19]:

$$m = \Delta \ln \sigma / \Delta \ln \dot{e}, \quad (1)$$

where $\sigma$ is the true stress.

The microstructure of the samples was studied by transmission electron microscopy (TEM) and X-ray diffraction analysis (XRD). The TEM method was used to measure the average grain size ($d_{av}$), the XRD method was used to measure the lattice parameter ($a$), average coherent scattering domain size ($D_{XRD}$), microdistortion level ($\langle \varepsilon^2 \rangle^{1/2}$) and dislocation density ($L_{dis}$) according to the relation [20]:

$$L_{dis} = 2\sqrt{3}\langle \varepsilon^2 \rangle^{1/2} / D_{XRD} b, \quad (2)$$

where $b = 0.286$ nm is the Burgers vector of dislocation in aluminium.

## 3. Experimental results and discussion

In the initial state, the Al−0.4Zr microstructure is characterized by elongated subgrains with an average length of $\sim 1800$ and a width of $\sim 1000$ nm [10]. Table 1 shows the main microstructure parameters of Al−0.4Zr in all states investigated herein. HPT treatment results in formation of a homogeneous UFG structure consisting of uniaxial grains with an average size of $d_{av} \approx 415$ nm (Figure 1, *a*). After UFG alloy annealing at 503 K, $d_{av}$ remains almost unchanged (Figure 1, *b*). Additional CR deformation results in slight increase of $d_{av}$ up to $\sim 490$ nm and increase of standard deviation of the average grain size ($\Delta d_{av}$) from 127 nm to 242 nm (Figure 1, *c*, Table 1). Thus, after annealing and small CR deformation, the change of the grain size is negligible.

XRD investigations has shown that the lattice parameter $a$ of the aluminium matrix is practically unchanged after annealing and additional deformations (Table 1) suggesting that Zr concentration in solid solution is almost unchanged by such treatments. UFG alloy annealing at 503 K results in reduction of dislocation density by a factor of $\sim 4$ (Table 1). Subsequent additional 3% CR deformation provides the increase of $L_{dis}$ up to the level typical for the HPT state. Additional 5% CR deformation without intermediate annealing ensures even higher increase of $L_{dis}$ up to $1 \cdot 10^{13}\,m^{-2}$. It has been shown before in [15] that the additional HPT deformation with 0.25−0.75 revolution after annealing at 503 K also results in increasing dislocation density up to the level typical for the sample before annealing (Table 1). Significant dependence of the average grain size and morphology on the degree of additional HPT deformation was not observed [15].

Figure 2 shows the stress-strain diagram obtained for Al−0.4Zr in initial state, after HPT treatment, post-annealing at 503K during 1 h and different types of additional deformation. Initial material has an yield strength of $\sigma_{0.2} \sim 122$ MPa, ultimate strength of $\sigma_{UTS} \sim 131$ MPa, high elongation to frature $\delta \sim 26\%$ and uniform elongation $\delta_1 \sim 4\%$ [15]. It can be seen that the HPT treatment results in increase of $\sigma_{UTS}$ up to $\sim 202$ MPa, while $\delta$ remains at sufficiently high level (Figure 2, Table 2). Post-annealing at 503 K during 1 h results in additional increase of $\sigma_{UTS}$ and $\sigma_{0.2}$ up to $\sim 252$ and $\sim 223$ MPa, respectively, but makes $\delta$ almost twice as low $\sim 13\%$. Hardening of UFG Al−0.4Zr alloy after annealing (annealing-induced hardening effect) was observed before [10] and was attributed to the relaxation of non-equilibrium grain boundaries followed by decreasing density of grain-boundary dislocations and possible formation of grain-boundary segregations and/or nanoclusters/nanoprecipitates [10]. GB relaxation during annealing of the UFG Al−0.4Zr alloy was observed *in situ* in a transmission electron microscope during such annealing directly in the microscope column [21].

Unlike the additional HPT deformation, additional 3% CR deformation after annealing ensures additional

**Table 1.** Microstructural analysis of Al−0.4Zr alloy in various states ($d_{av}$ is the average grain size, $a$ is the lattice parameter, $D_{XRD}$ is the coherent scattering domains size, $\langle\varepsilon^2\rangle^{1/2}$ is the lattice microdistortion level, $L_{dis}$ is the dislocation density)

| State | TEM data | | XRD data | | | |
|---|---|---|---|---|---|---|
| | $d_{av}$, nm | $\Delta d_{av}$, nm | $a$, Å | $D_{XRD}$, nm | $\langle\varepsilon^2\rangle^{1/2} \cdot 10^{-4}$ | $L_{dis} \cdot 10^{12}$, m$^{-2}$ |
| HPT | 415 ± 19 | 197 | 4.0505 ± 0.0001 | 570 ± 15 | 2.5 ± 0.2 | 5.2 |
| HPT_AN | 395 ± 12 | 127 | 4.0512 ± 0.0001 | 815 ± 15 | 0.9 ± 0.2 | 1.4 |
| HPT_AN_CR3% | 490 ± 32 | 242 | 4.0512 ± 0.0001 | 500 ± 11 | 3.0 ± 0.1 | 7.3 |
| HPT_CR5% | – | – | 4.0507 ± 0.0001 | 361 ± 7 | 2.95 ± 0.1 | 9.9 |
| HPT_AN_0.25HPT [15] | 318 ± 30 | 200 | 4.0515 ± 0.0001 | 495 ± 10 | 2.2 ± 0.1 | 5.4 |
| HPT_AN_0.75HPT [15] | – | – | 4.0509 ± 0.0001 | 490 ± 13 | 2.3 ± 0.1 | 5.7 |

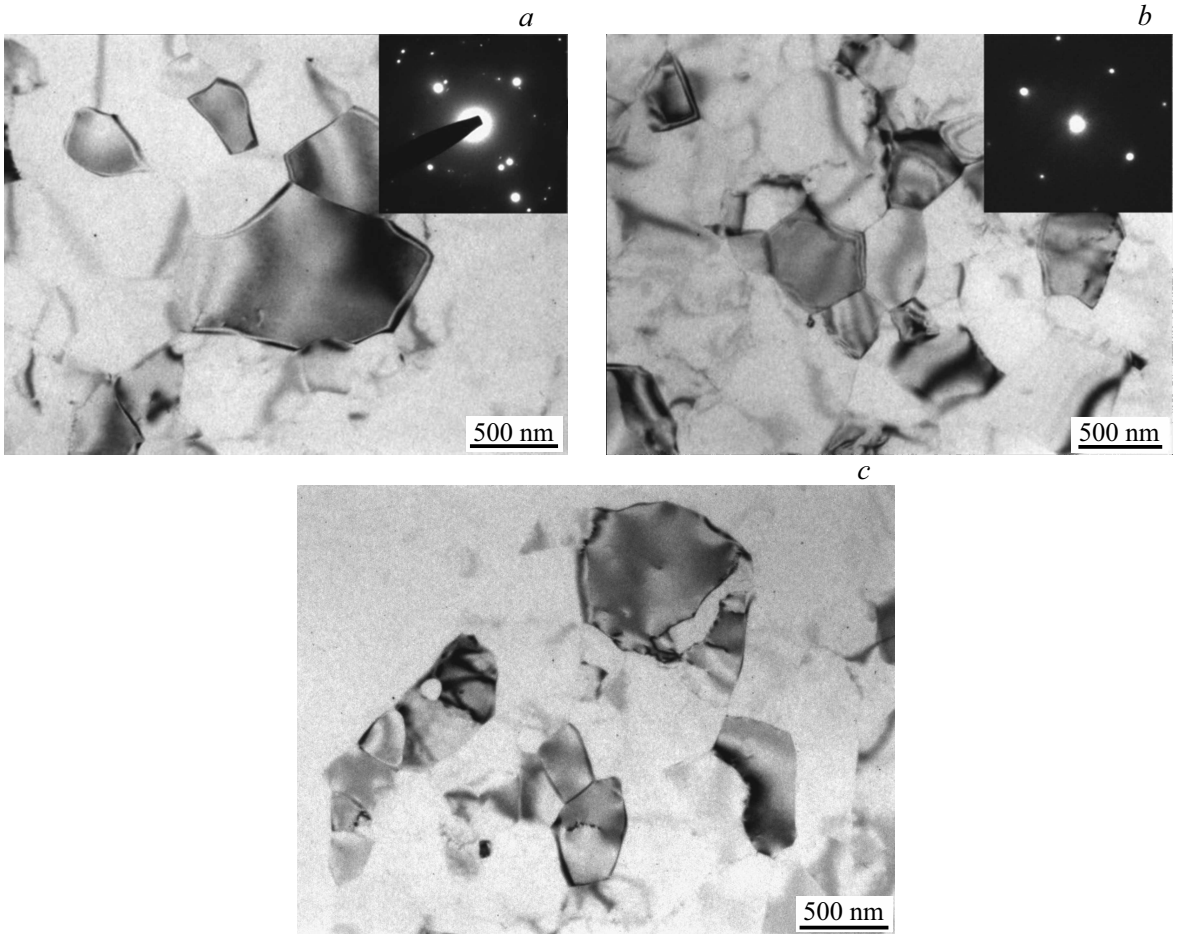


**Figure 1.** Al−0.4Zr alloy microstructure after HPT treatment ($a$), additional annealing at 503 K during 1 h ($b$) and subsequent additional 3% cold rolling deformation($c$).

hardening: $\sigma_{0.2}$ and $\sigma_{UTS}$ increase up to $\sim 251$ and $\sim 275$ MPa, respectively, however, plasticity decreases to very low values $\delta \leq 2\%$ (Table 2). In this case, the alloy behaves as coarse-grain materials for which strain hardening is typical. Mechanical properties of the UFG alloy are almost independent on the degree of rolling (Figure 2, Table 2). It should be noted that increase of $\sigma_{0.2}$ ensured by 3% CR is equal to $\Delta\sigma_{0.2} \approx 28$ MPa (Table 2) and may be associated with additional strain hardening due to the introduction of additional density of lattice dislocations into the grain body by rolling. Recently, the high resolution scanning transmission electron microscopy (STEM) has shown that such deformation after short-term low-temperature annealing ensures formation of a well-developed dislocation structure inside grains in UFG Al (99.7%) structured by HPT in similar condition [22]. Under the TEM resolution conditions used herein, occurrence of individual dislocations and dislocation walls was observed

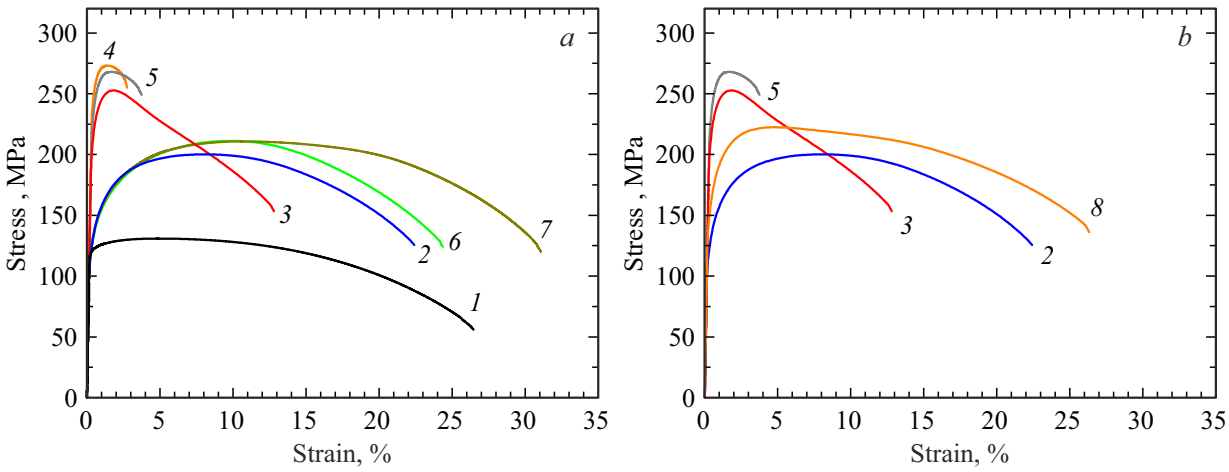


**Figure 2.** Stress–strain diagrams for Al–0.4Zr samples in various states: initial (curve *1*), after HPT treatment (curve *2*), post-annealing at 503 K (curve *3*), post-annealing at 503 K and additional 3% and 5% cold rolling deformation (curves *4* and *5*) and HPT with 0.25 and 0.75 (curves *6* and *7*, data of [15]), after additional 5% cold rolling deformation without intermediate annealing (curve *8*). *a*) curves *1–7*; *b*) curves *2, 3, 5, 8*.

**Table 2.** Mechanical properties of Al–0.4Zr in different structural states ($\sigma_{0.2}$ is the yield strength, $\sigma_{UTS}$ is the ultimate strength, $\delta$ is the elongation to fracture, $\delta_1$ is the uniform elongation)

| State | $\sigma_{0.2}$, MPa | $\sigma_{UTS}$, MPa | $\delta$, % | $\delta_1$, % |
|---|---|---|---|---|
| HPT | 130 ± 1 | 202 ± 1 | 22 ± 1 | 8.3 ± 0.7 |
| HPT_AN | 223 ± 2 | 252 ± 1 | 13 ± 1 | 1.5 ± 0.1 |
| HPT_AN_CR3% | 251 ± 2 | 275 ± 2 | 2 ± 1 | 0.9 ± 0.1 |
| HPT_AN_CR5% | 237 ± 8 | 268 ± 1 | 3 ± 1 | 1.5 ± 0.3 |
| HPT_CR5% | 167 ± 2 | 223 ± 1 | 26 ± 1 | 4.5 ± 0.5 |
| HPT_AN_0.25HPT [15] | 131 ± 3 | 213 ± 2 | 24 ± 1 | 9.4 ± 0.1 |
| HPT_AN_0.75HPT [15] | 133 ± 2 | 210 ± 1 | 30 ± 1 | 10 ± 1 |

inside grains in HPT_AN_CR3% samples (Figure 1, *c*), however, more detailed study of the distribution of rolling-induced dislocations requires systematic STEM study.

It has been shown earlier in [15] that additional HPT with 0.25–0.75 revolution after annealing ensures reduction of $\sigma_{UTS}$ and $\sigma_{0.2}$ to ~ 213 and ~ 131 MPa, respectively, and to increase of $\delta$ and $\delta_1$ up to the values typical for for the state before annealing and even higher values. Such behavior was attributable to the additional density of dislocations introduced into the structure of GB relaxed by annealing that enhanced the degree of non-equilibrium and, thus, facilitated dislocation emission from GB and implementation of plastic flow under loading [15]. Increasing density of dislocations resulting from small additional HPT after annealing was observed experimentally (Table 1) [15].

Thus, the additional deformation of the UFG alloy annealed at 503 K by two different methods (HPT and CR) ensures comparable increase in the density of dislocations (Table 1), but to the opposite changes of the mechanical properties (Table 2) that is most probably attributable to the different distribution of the induced additional density of dislocations in the UFG structure: preferably in GB in the HPT_AN_0.25/0.75HPT samples [15] and preferably within grains in the HPT_AN_CR3% samples. Such difference in dislocation distribution may be attributed to the different deformation conditions when both deformation methods are implemented (degree and rate of strain, type of stress-strain state) [22]. Additional deformation conditions and degree of deformation are different in CR and HPT methods. In the former case, compression deformation is carried out in plane stress conditions. In the latter case, shear deformation is performed in quasi-hydrostatic pressure conditions. This may result in activation of different slip systems in cases of additional HPT and CR deformation. Strain values for various types of loading may be compared using the Von Mises equivalent strain ($\varepsilon_{eq}$) evaluation [23] that has shown that 10-revolution HPT processing ensures $\varepsilon_{eq} \approx 181$ at a distance of 5 mm from the disc center (i. e. within the sample test length). In the case of additional 0.25-revolution by HPT deformation and 3% CR deformation, the equivalent strain is equal to $\varepsilon_{eq} \approx 4.5$ and $\varepsilon_{eq} \approx 0.033$, respectively.

To verify the defining role of the non-equilibrium GB state in the achievement of high plasticity, additional uniaxial

tension test of the UFG Al−0.4Zr alloy was carried out after additional CR deformation without intermediate annealing (Figure 2, *b*, curve HPT_CR5%). In this case, the additional deformation ensured the increase of $\sigma_{0.2}$ by $\sim 37$ MPa and of $\sigma_{UTS}$ by $\sim 21$ MPa, and the plasticity also increased a little (Table 2). Thus, combined strain treatment by the HPT method followed by cold rolling (HPT_CR5% state) ensured both increased strength and increased plasticity compared with the HPT state. The achieved increased strength may be attributable to the increased density of lattice dislocations after post-HPT cold rolling (Table 1). The increased plasticity with increasing strength is an unusual phenomenon. First, the achieved high plasticity of the HPT_CR5% samples, unlike the HPT_AN_CR5% samples, suggests that plasticity in the UFG structure with relaxed GB (equilibrium or near-equilibrium after annealing) is much lower than in the samples with non-equilibrium grain boundaries. Increased plasticity in the HPT_CR5% state compared with the HPT state (GBs are non-equilibrium in both states) may be associated with the fact that additional CR introduces additional density of dislocations preferably into the grain body [22]. Dislocations introduced by rolling will limit the mean free path of dislocations emitted from GB and, thus, will facilitate strain hardening. Actually, the strain hardening rate (coefficient) $\theta = d\sigma/d\varepsilon$ at the early deformation stage is higher for the HPT_CR5% state than for the HPT state (Figure 3), that, according to the Conside're criterion [23], delays the strain localization moment and necking and, therefore, results in increased plasticity.

It is known that grain boundary sliding (GBS) contributes to the total plasticity of HPT-structured UFG Al [24,25]. GBS activation facilitates more homogeneous microplastic flow in the sample that prevents the macrolocalization and necking processes, thus, facilitating the increased plasticity. GBS activation is followed by the increase of strain rate sensitivity coefficient [25].

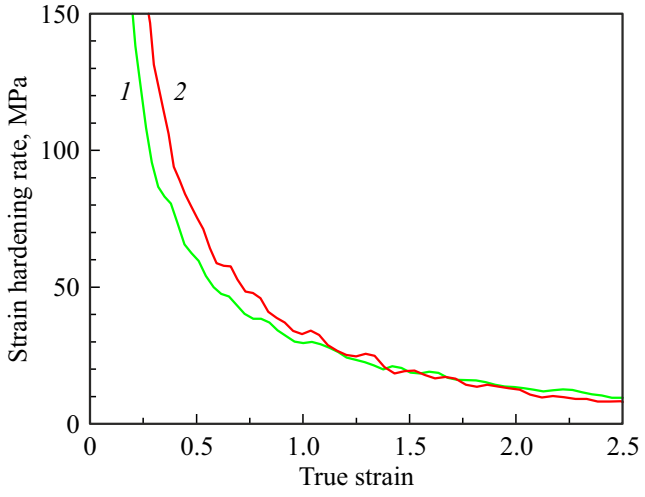


**Figure 3.** Strain hardening rate vs. the degree of strain for Al−0.4Zr in HPT (curve *1*) and HPT_CR5% states (curve *2*).

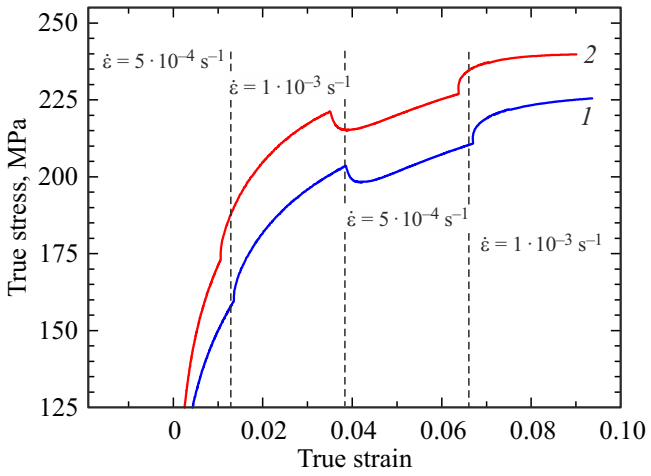


**Figure 4.** Strain-rate jump test at a base rate of $5 \cdot 10^{-4}$ s$^{-1}$ for Al−0.4Zr samples in the HPT (curve *1*) and HPT_CR5% (curve *2*) states.

Figure 4 shows the results of strain-rate jump test for the HPT [15] and HPT_CR5% samples. The strain-rate sensitivity coefficient $m$ is equal to $\sim 0.045$ for both HPT and HPT_CR5% states that is identical to $m$ values for the HPT and HPT_AN_0.25HPT states determined earlier [14]. Therefore, increased plasticity in the HPT_CR5% state is not attributable to any intensification of GBS, because the latter is generally followed by the increase of $m$.

## 4. Conclusion

The study investigates the effect of a small additional CR deformation on the mechanical properties of the HPT-structured UFG Al−0.4Zr alloy. It is shown that, unlike the additional HPT, the additional 3−5% CR deformation after preliminary low-temperature annealing does not result in the plasticization effect in the UFG Al−0.4Zr alloy, but rather reduces the plasticity to $\sim 2\%$ and slightly increases the yield strength by 6−12%, that is most probably caused by the additional density of dislocations introduced by rolling preferable into the grain body. The findings support the concept that non-equilibrium GBs play the key role in the increase of plasticity due to additional deformation with strength retention at a high level.

It is shown that the additional CR deformation without preliminary annealing results in simultaneous increase of strength (yield strength by $\sim 30\%$ and ultimate tensile strength by $\sim 10\%$), while the plasticity also increases a little and achieves $\sim 26\%$, that is attributable to the increased strain hardening rate due to the introduction of additional density of dislocations into the grain body in the UFG structure with non-relaxed grain boundaries.

The offered approach involving simultaneous strength and plasticity increase may be probably also applicable for some other aluminum alloys provided that the proper microstructure parameters are achieved.

Strain-rate sensitivity coefficients for the UFG alloy before and after additional 5% cold rolling deformation were determined. They were the same and equal to $m \approx 0.045$ that excludes the increase of grain boundary sliding contribution to the total plasticity after additional cold rolling deformation.

### Conflict of interest

The authors declare that they have no conflict of interest.

## References


[1] D.I. Belyi. Kabeli i provoda **332**, *1*, 8 (2012). (in Russian). https://www.elibrary.ru/item.asp?id=18852363

[2] F.R. Ismagilov, R.G. Shakirov, N.K. Potapchuk, T.Yu. Volkov. Osnovnye voprosy proektirovaniya vozdushnykh linii elektroperedach. Uch. posobie. 2-e izd. Mashinostroenie, M. (2015). 211 p. (in Russian).

[3] R.Z. Valiev, A.P. Zhilyaev, T.G. Langdon, Ob'emnyie nanostrukturnye materialy: fundamental'nye osnovy i primeneniya. Eko-Vektor, SPb (2017). 479 p. (in Russian).

[4] I.A. Ovid'ko, R.Z. Valiev, Y. T. Zhu. Prog. Mater. Sci. **94**, 462 (2018). https://doi.org/10.1016/j.pmatsci.2018.02.002

[5] K.E. Knipling, D.C. Dunand, D.N. Seidman. Acta Mater. **56**, *1*, 114 (2008). https://doi.org/10.1016/j.actamat.2007.09.004

[6] N.A. Belov, A.N. Alabin, A.R. Teleuova. Met. Sci. Heat Treat. **53**, 455 (2012). https://doi.org/10.1007/s11041-012-9415-5

[7] W.W. Zhou, B. Cai, W.J. Li, Z.X. Liu, S. Yang. Mater Sci. Eng. A **552**, 353 (2012). https://doi.org/10.1016/j.msea.2012.05.051

[8] N.A. Belov, N.O. Korotkova, T.K. Akopyan, V.N. Timofeev. JOM **72**, *4*, 1561 (2020). https://doi.org/10.1007/s11837-019-03875-0

[9] D.S. Voroshilov, M.M. Motkov, S.B. Sidelnikov, R.E. Sokolov, A.V. Durnopyanov, I.L. Konstantinov, V.M. Bespalov, T.V. Bermeshev, I.S. Gudkov, M.V. Voroshilova, Y.N. Mansurov, V.A. Berngardt. Int. J. Lightweight Mater. **5**, *3*, 352 (2022). https://doi.org/10.1016/j.ijlmm.2022.04.002

[10] T.A. Latynina, A.M. Mavlyutov, M.Yu. Murashkin, R.Z. Valiev, T.S. Orlova. Phil. Mag. **99**, *19*, 2424 (2019). https://doi.org/10.1080/14786435.2019.1631501

[11] T.S. Orlova, T.A. Latynina, A.M. Mavlyutov, M.Y. Murashkin, R.Z. Valiev. J. Alloys Compd. **784**, 41 (2019). https://doi.org/10.1016/j.jallcom.2018.12.324.

[12] M.Yu. Murashkin, A.E. Medvedev, V.U. Kazykhanov, G.I. Raab, I.A. Ovid'ko, R.Z. Valiev. Rev. Adv. Mater. Sci. **47**, 16 (2016). https://www.ipme.ru/e-journals/RAMS/no_14716/03_14716_murashkin.pdf

[13] T.S. Orlova, T.A. Latynina, M.Yu. Murashkin, V.U. Kazykhanov. FTT **61**, *12*, 2447 (2019). (in Russian). https://doi.org/10.21883/FTT.2019.12.48582.558

[14] A. Mohammadi, N.A. Enikeev, M.Yu. Murashkin, M. Arita, K. Edalati. Acta Mater. **203**, 116503 (2021). https://doi.org/10.1016/j.actamat.2020.116503

[15] T.S. Orlova, A.M. Mavlyutov, M.Y. Murashkin, N.A. Enikeev, A.D. Evstifeev, D.I. Sadykov, M.Yu. Gutkin. Materials **15**, *23*, 8429 (2022). https://doi.org/10.3390/ma15238429

[16] A.M. Mavlyutov, T.A. Latynina, M.Yu. Murashkin, R.Z. Valiev, T.S. Orlova. FTT **59**, *10*, 1949 (2017). (in Russian). http://dx.doi.org/10.21883/FTT.2017.10.44964.094

[17] T.S. Orlova, N.V. Skiba, A.M. Mavlyutov, M.Yu. Murashkin, R.Z. Valiev, M.Yu. Gutkin. Rev. Adv. Mater. Sci. **57**, *2*, 224 (2018). https://doi.org/10.1515/rams-2018-0068

[18] N.V. Skiba, T.S. Orlova, M.Yu. Gutkin. Phys. Solid State **62**, *11*, 2094 (2020). https://doi.org/10.1134/S1063783420110347

[19] I. Sabirov, Y. Estrin, M.R. Barnett, I. Timokhina, P.D. Hodgson. Scr. Mater. **58**, *3*, 163 (2008). https://doi.org/10.1016/j.scriptamat.2007.09.057

[20] G.K. Williamson, R.E. Smallman. Phil. Mag. **1**, *1*, 34 (1956). https://doi.org/10.1080/14786435608238074

[21] W. Lefebvre, N.V. Skiba, F. Chabanais, M.Yu. Gutkin, L. Rigutti, M.Yu. Murashkin, T. S. Orlova. J. Alloys Compd., **862**, *5*, 158455 (2021). https://doi.org/10.1016/j.jallcom.2020.158455

[22] T.S. Orlova, D.I. Sadykov, D.A. Kirilenko, A.I. Lihachev, A.A. Levin. Mater. Sci. Eng. A **875**, 145122 (2023). https://doi.org/10.1016/j.msea.2023.145122

[23] G.E. Dieter. Mechanical Metallurgy. McGraw-Hill, Boston (1961). 615 p.

[24] N.Q. Chinh, T. Csanádi, T. Györi, R.Z. Valiev, B.B. Straumal, M. Kawasaki, T.G. Langdon. Mater. Sci. Eng. A **543**, 117 (2012). https://doi.org/10.1016/j.msea.2012.02.056

[25] K.V. Ivanov, E.V. Naydenkin. Mater. Sci. Eng. A *23*, 8429 (2022). https://doi.org/10.3390/ma15238429


*Translated by E.Ilyinskaya*